# PROCEEDINGS OF SPIE

SPIEDigitalLibrary.org/conference-proceedings-of-spie

# Illuminating the optical properties of an LED-based spectral light source for hyperspectral endoscopy

Browning, Craig, Parker, Marina, Rich, Thomas, Leavesley, Silas

Craig M. Browning, Marina Parker, Thomas C. Rich, Silas J. Leavesley, "Illuminating the optical properties of an LED-based spectral light source for hyperspectral endoscopy," Proc. SPIE 11636, Optical Biopsy XIX: Toward Real-Time Spectroscopic Imaging and Diagnosis, 1163608 (5 March 2021); doi: 10.1117/12.2583228



Event: SPIE BiOS, 2021, Online Only

# Illuminating the optical properties of an LED-based spectral light source for hyperspectral endoscopy

Craig M. Browning<sup>1,2</sup>, Marina Parker<sup>1,2</sup>, Thomas C. Rich<sup>3,4</sup>, Silas J. Leavesley<sup>1,3,4</sup>
<sup>1</sup>Chemical and Biomolecular Engineering, University of South Alabama, AL 36688
<sup>2</sup>Systems Engineering, University of South Alabama, AL 36688
<sup>3</sup>Pharmacology, University of South Alabama, AL 36688
<sup>4</sup>Center for Lung Biology, University of South Alabama, AL 36688

#### **ABSTRACT**

In the United States, the gold standard for endoscopic screening is white light endoscopy (WLE) which uses a singular broad spectrum light source to illuminate the colorectum. However, WLE provides minimal contrast to small, flat or early growth lesions compared to the surrounding mucosa, in turn, increasing the miss rate of these lesions allowing for further growth of potentially fatal cancer (colorectal cancer is the 3<sup>rd</sup> highest risk cancer). The most notable addition to endoscopy is narrow-band imaging (NBI) illuminating with two specific bandwidths of blue and green light to enhance the vascular structures through absorption. NBI provides enhanced contrast but minimal improvements in detection accuracy. A logical extension of NBI would be to use more than 2 wavelength bands to generate contrast. We propose an LED-based spectral light source to provide hyperspectral imaging for the potential of enhancing endoscopic images. This would provide 8+bandwidths of light plus the potential of fluorescence, doubling the possible information content of enhanced images. Here, we report on improved illumination throughput, initial resolution testing and color testing for a previously reported prototype LED-based spectral light source. Results show that, while optical transmission is low, spectral illumination is still possible when combined with high-power LED emitters. Resolution results are compared to the gold standard white light source and color testing results provide baseline validation for the spectral output of the system. These results provide benchmark data for evaluating the potential of hyperspectral imaging for enhanced endoscopic imagery.

**Keywords:** Endoscopy, Colonoscopy, Colorectal Cancer, Light Emitting Diode, Spectroscopy, Hyperspectral Imaging, Light Guides, Optical Pathways

# 1. INTRODUCTION

Videos or motion pictures have saturated human life from entertainment in movies to recording scientific discoveries to present day where basic interactions are conducted with video conferences amid a pandemic. Interestingly, motion pictures development consisted of milestones oscillating between entertainment and scientific use. The use of the motion picture begins with hand crafted, hand spun animation wheels for optical illusion toys such as the phenakistiscope (1830's). After the invention of film, physiologist Etienne-Jules Marey recorded animal movements (1880's) using chronophotography (serial photography) with the "photographic gun" invention capturing short (12 fps) videos. <sup>2,3</sup> A decade later, William K.L. Dickson invented the Kinetograph, the first motorized (40 fps) cameras and projectors, for the silent film entertainment era. 4,5 Videos on film were the mainstay until the current digital era which allows for high definition and high framerate possibilities. Pictures in motion have provided numerous avenues of entertainment and a wealth of knowledge for the sciences. Future advancements aim to provide more depth to a video or information in the case of science. The goal of this manuscript is to highlight a potential source of video data that could advance fields such as microscopy and endoscopy. The emphasis here is spectroscopic analysis through reflectance and fluorescence imaging. Microscopy has provided insight to the world too small for the naked eye to perceive and endoscopy has done the same for hollow cavities of the human body. The basis for illumination in each platform, was a broadband white light source to illuminate the region and provide the reflected image in return. Multiple fluorescence microscopy techniques have since been that provide improved performance for a range of parameters, such as resolution, 3-dimensional imaging, etc. STORM/PALM (Stochastic Optical Reconstruction Microscopy/Photoactivated Localization Microscopy) provides super resolution images at the expense of increased scan times. Wide-field and confocal microscopy provide quasi-real time images at the cost of lower resolution. Light sheet microscopy is a newer technique that allows a comparable or improved field of view to wide-field microscopy while also allowing 3-dimensional and time-lapse capabilities. However, many of

Optical Biopsy XIX: Toward Real-Time Spectroscopic Imaging and Diagnosis, edited by Robert R. Alfano Stavros G. Demos, Angela B. Seddon, Proc. of SPIE Vol. 11636, 1163608 ⋅ © 2021 SPIE CCC code: 1605-7422/21/\$21 ⋅ doi: 10.1117/12.2583228

these advanced microscopy techniques come at the expense of increased acquisition times, prohibiting high-speed imaging or rapid screening of wide sections of tissue. Endoscopy has also benefitted from technological advances, including the development of narrow-band imaging (NBI) and autofluorescence imaging (AFI). NBI takes advantage of the absorption of blue and green illumination in the blood vessels to provide enhanced contrast of the vasculature as indicated by darker or blue-colored pixels. Autofluorescence imaging uses similar bands of light to acquire the endogenous fluorescence of tissue, usually indicating vascular density. Unfortunately, neither option has provided sufficient enhancements for optical diagnoses<sup>6,7</sup>, such as to become the new gold standard of endoscopy screenings.

The spectroscopic modalities mentioned above tend to use 1-4 spectral channels (lower spectral resolution), however, there are potential visual enhancements with increased spectral resolution. Literature provides numerous studies of endogenous fluorophores which occur in human tissue that could be utilized to provide contrast enhancements in imaging, notably to contrast differences between normal and cancerous tissue. Imaging of collagen (excitation at 350 nm) and elastin (excitation at 360 nm) in the extracellular matrix could reveal irregularities in the matrix with a potential correlation to tumor growth. Reduced nicotinamide adenine dinucleotide (NADH) and flavin adenine dinucleotide (FAD) have excitation peaks ranging from 365 nm to 488 nm that can be used to estimate metabolism via calculation of a redox ratio. Areas of higher metabolic activity may correlate to tumor invasion. Protoporphyrin IX (PPIX) is a precursor to hemoglobin and tends to accumulate in tumor growth regions accounting for leeching of nutrients from the bloodstream (excites at 405 nm). There are multiple exogenous fluorophores that have been created to aid in the visualization of cellular phenomena by binding to proteins, calcium and glycosaminoglycans. However, the scope of this work focuses on detection of reflectance markers (e.g. vasculature absorbance as mentioned using narrow-band) and endogenous fluorophores. The potential information from a mixture of reflectance and autofluorescence data could enhance the fields of microscopy and endoscopy. Hence, there is a need for an imaging modality which provides an optimal balance of spatial and spectral resolution at video rate acquisitions.

We believe that hyperspectral imaging (HSI) could provide a solution to acquire spectroscopic reflectance and autofluorescence endoscopy data at video-rate speed. The resulting image from HSI is a two-dimensional image acquired over a range of wavelength intervals creating a three-dimensional hypercube which provides a unique spectrum for every pixel. This technique is most notably used in remote sensing which traditionally filters reflected sunlight through various band-pass filters on a detector providing spectroscopic data for satellite images, agricultural and archaeological analysis.<sup>19,20</sup> Other small-scale examples include food processing and historical document restoration using similar techniques with a broadband light source. 21,22 Examples of the fluorescence hyperspectral imaging have been documented for agricultural, endoscopic and microscopic settings.<sup>23–25</sup> The traditional approach for performing HSI with fluorescence has been to illuminate the sample with one or several wavelength bands for excitation and spectrally filter the emitted light using a filter wheel, tunable filter, or diffractive optical element. However, we have demonstrated that a new approach of filtering the fluorescence excitation using a tunable filter, while acquiring fluorescence emission images using a broad band- or long-pass emission filter, can allow for HSI fluorescence imaging with improved signal strength. The reduced filtering resulted in a 5-20 fold increase in signal to noise ratio (SNR) and decreased acquisition times from 3 s to 300 ms.<sup>26</sup> However, this version of HSI provided spectroscopic data at ~3 fps (frames per second) when the standard video rate is 24 fps. The limitation was primarily due to the time required for the mechanical switching of the band-pass filters for the excitation source. More recently, we have developed a fluorescence excitation-scanning spectral imaging system using an array of wavelength specific LEDs with combining optics to a common output in place of the broadband light source used previously. This decreases the excitation switching speeds through electronic switching of the LEDs. This LED-based light source has been coupled to an endoscopic platform to test the feasibility of real-time reflectanceautofluorescence hyperspectral imaging. We have previously presented initial irradiance data of the light source and example images through an endoscope. 27-29 The resulting system can achieve video rate speeds at the expense of adequate or distinguishable spatial resolution. The trade-off between resolution and acquisition speeds has motivated us to optimize irradiance transmission.<sup>30</sup> However, we also need to develop metrics for quantitative bench testing and comparison between subsequent iterations of hyperspectral endoscopic systems. Here, we present a brief discussion of the continuing optimization in concurrence with testing the basic abilities of the system. Metrics include transmission of optics throughout the light path and comparison to datasheets, if applicable and fluorescent feasibility testing.

#### 2. METHODS

The benchtop testing protocol detailed below was used to characterize the performance of a hyperspectral endoscope system. Results can be used to evaluate system limitations and provide a standardized approach for testing as newer iterations are developed.

# 2.1 System Upgrades

The proof-of-concept LED-based endoscopic light source was designed and assembled for feasibility benchtop testing as described previously.<sup>27–29</sup> As part of the initial prototyping effort, some components were underspecified for safety and accessibility for the end product (ability to be easily modified). For example, each LED is controlled via a separate current line with a respective current driver controlled by individual digital and analog signal lines. The current drivers installed (RCD-24-0.35, RECOM Power GmbH) provided a maximum of 350 mA of power to each LED. This power level was selected to reduce the risk of overpowering or damaging an LED while connecting and testing electric lines. Upon review of the LED's respective specification sheets (SMB1N-xxxx-xx, Marubeni America Co.) the LEDs used in this design had a varying forward current range rated from 350 mA to 1 A. Hence, to maximize the irradiance output, we replaced the original current drivers with 1 A current drivers. The current drivers are controlled with a reference voltage range allowing accurate and constant current for the LED. The reference voltage controller allowed us to measure the voltage drop across the single resistor in line to the LED and accurately calculate the amperage supplied to the LED. To minimize damage to the LEDs, the current supplied was specified to be 95% of the respective maximum forward current, as listed on the specification sheet. The current drivers were controlled through the system interface software (Nikon Elements, Nikon Instruments Inc.). The irradiance of each LED was measured within the reference current boundaries and compared to the data sheet and previous irradiance measurements using the original current drivers. Irradiance measurements were acquired using a spectrometer (QE65000, Ocean Optics) and integrating sphere (RT-060-SF, Labsphere) calibrated to a NISTtraceable response using a standardized light source (LS-1-CAL, Ocean Optics). Irradiance measurements were also acquired through the multi-furcated solid light guide (the combining optics for this light source) and the light guide + endoscope to calculate the transmission and compare to previous data. 27,29,31

# 2.2 Filter Transmission & Fluorescence Imaging

The majority of optical testing focused on the LEDs and multi-furcated solid light guide. However, there are other optical components within the light path to the detector. One is the long-pass emission filter placed before the camera at the proximal end of the endoscope. When the filter is absent, reflectance images are acquired. When the filter is in place, fluorescence images are acquired. Therefore, we measured the transmission of several available filters for potential use when performing fluorescence imaging. Transmission measurements were acquired with the QE65000 spectrometer and a cuvette/filter holder (CUV, Ocean Optics) illuminated by a broadband light source (LS-1-CAL, Ocean Optics). This same setup was used to measure the transmission of a set of plastic fluorescence reference slides (FSK5, ThorLabs Inc.). The slide set included a blue, green, yellow, orange and red fluorescent slide.

LEDs were selected for illumination depending on the filter selected for the excitation-emission cut-off. The distal end of the endoscope was matched with a fluorescent filter (~1-2 mm separation) and an image was acquired. This was repeated for every fluorescent slide and every band-pass filter measured. Image intensities were measured through the imaging software (Nikon Elements), from regions of interest on the image providing arbitrary intensity as a function of the excitation sources (LEDs). The data from each fluorescent slide was combined to compare the effects of changing the emission filter cut-off wavelength.

#### 3. RESULTS AND DISCUSSION

The following is a summary of irradiance and transmission results acquired through the optical characterization steps described above.

#### 3.1 LED Irradiance

Each LED electrical circuit was updated with a 1 A current driver (from a 350 mA driver) to provide sufficient amperage to all LEDs for illumination. Boundaries were set, in software, so the maximum current flowing to each LED was no more than 95% of the rated forward current. The irradiance was measured for each LED at the new maximum current to compare radiant power (mW) with respect to the original setup. Measurements were repeated for each LED through the multifurcated light guide and through the light guide + endoscope. The measurements were compared to the irradiance through the original setup (with the 350 mA current drivers) to show irradiance differences.

Table 1: Irradiance data for raw optical power from the LEDs used in the hyperspectral endoscopic system, power transmitted through the light guide and power transmitted through the light guide + endoscope. Transmission through the light guide and light guide + endoscope were calculated by dividing the radiant power output by the raw radiant power of the LED. The Original section of the table is the irradiance data using the 350 mA current drivers and the Updated section is the irradiance data using 1 A current drivers supplying 95% of the maximum rated current for each LED. The bottom section of the table (Comparison) calculates the percentage change in radiant power for each position measured as the ratio of (the difference between the Updated data and the Original data) divided by the Original data.

Original																
Wavelength (nm)	365	405	420	450	470	490	525	590	620	670	680	750	810	850	940	980
LED (mW)	212.62	387.78	370.35	354.04	294.67	235.13	184.11	106.23	167.2	257.54	76.897	102.63	145.67	193.53	153.09	30.536
Lightpipe (mW)	0.00	1.98	7.55	4.38	4.63	1.61	4.31	1.27	1.71	10.90	0.67	2.12	2.50	6.28	1.50	0.35
Endoscope (mW)	0.000	0.003	0.026	0.016	0.023	0.008	0.041	0.011	0.009	0.091	0.003	0.014	0.016	0.055	0.014	0.001
% Transmission through Lightpipe	0.00%	0.51%	2.04%	1.24%	1.57%	0.69%	2.34%	1.19%	1.02%	4.23%	0.87%	2.06%	1.72%	3.25%	0.98%	1.14%
% Transmission through Endoscope	0.00%	0.00%	0.01%	0.00%	0.01%	0.00%	0.02%	0.01%	0.01%	0.04%	0.00%	0.01%	0.01%	0.03%	0.01%	0.00%
Updated																
LED (mW)	393.90	662.49	451.82	404.59	348.30	261.88	209.10	122.00	196.53	517.88	145.51	273.03	340.45	630.76	456.32	113.40
Lightpipe (mW)	0.00	2.93	8.56	5.02	5.48	1.80	4.93	1.53	2.04	22.75	1.32	6.12	6.78	20.30	4.31	0.55
Endoscope (mW)	0.000	0.006	0.026	0.016	0.023	0.008	0.039	0.012	0.010	0.163	0.005	0.036	0.037	0.135	0.009	0.006
% Transmission through Lightpipe	0.00%	0.44%	1.89%	1.24%	1.57%	0.69%	2.36%	1.25%	1.04%	4.37%	0.91%	2.24%	1.99%	3.22%	0.94%	0.48%
% Transmission through Endoscope	0.00%	0.00%	0.01%	0.00%	0.01%	0.00%	0.02%	0.01%	0.00%	0.03%	0.00%	0.01%	0.01%	0.02%	0.00%	0.01%
Comparison																
LED	85%	71%	22%	14%	18%	11%	14%	15%	18%	101%	89%	166%	134%	226%	198%	271%
Lightpipe	0%	48%	13%	15%	19%	11%	14%	20%	19%	109%	97%	189%	171%	223%	188%	57%
Endoscope	0%	134%	1%	1%	1%	-1%	-4%	2%	9%	79%	101%	157%	130%	146%	-38%	418%

The LED comparison corresponds to what we expected to see, which was an increase in irradiance output ranging from 11% to 271%. The same trend was observed in the Lightpipe comparison, however, lower increases due to transmission losses through the multibranched optic, ranging from 0% - 223%. The Endoscope comparison provided a slightly different perspective with a few wavelength channels that underperformed with the updated current drivers compared to the original. The smaller increases were to be expected with reduced intensity through the endoscope. Two of the three channels (490 nm and 525 nm) that had decreases were small enough changes to be negligible. The 940 nm channel had a 38% decrease between the setups, however, it is one of the lowest transmitting IR LEDs so the decrease was also negligible. The IR LEDs overall had the most significant increase and this was a direct correlation to the updated current drivers. These infrared channels were originally only supplied ~ 320 mA of current while they are rated for 600-1000 mA. It should be noted that the comparison of transmission between the setups present similar throughputs. Therefore, even though the LEDs were increased to "full" potential, the increased output through the light guide or endoscope resulted in comparable % transmission. These results point toward a need for continued optimization of the combining optics to increase transmission.

## 3.2 Endoscopic LED-based Fluorescence

Fluorescence imaging on a microscope platform is usually implemented through a dichroic filter cube with band-pass or band-pass filters for the excitation, a long-pass dichroic beamsplitter, and long-pass or band-pass filters for the emission. The LED-based endoscope system provides narrow-band excitation and allows for the omission of the band-pass filters on the excitation side. Hence, only a single band-pass or long-pass filter is needed on the emission. Here, we tested a few off-the-shelf filter options to assess the effect of emission filter on spectral imaging performance. The transmission spectrum of each emission filter was measured to assess bandwidth, transmission, and out-of-band rejection for each of 3 filters: 450/20 nm band-pass filter, 488/15 nm band-pass filter, 570 nm long-pass filter.

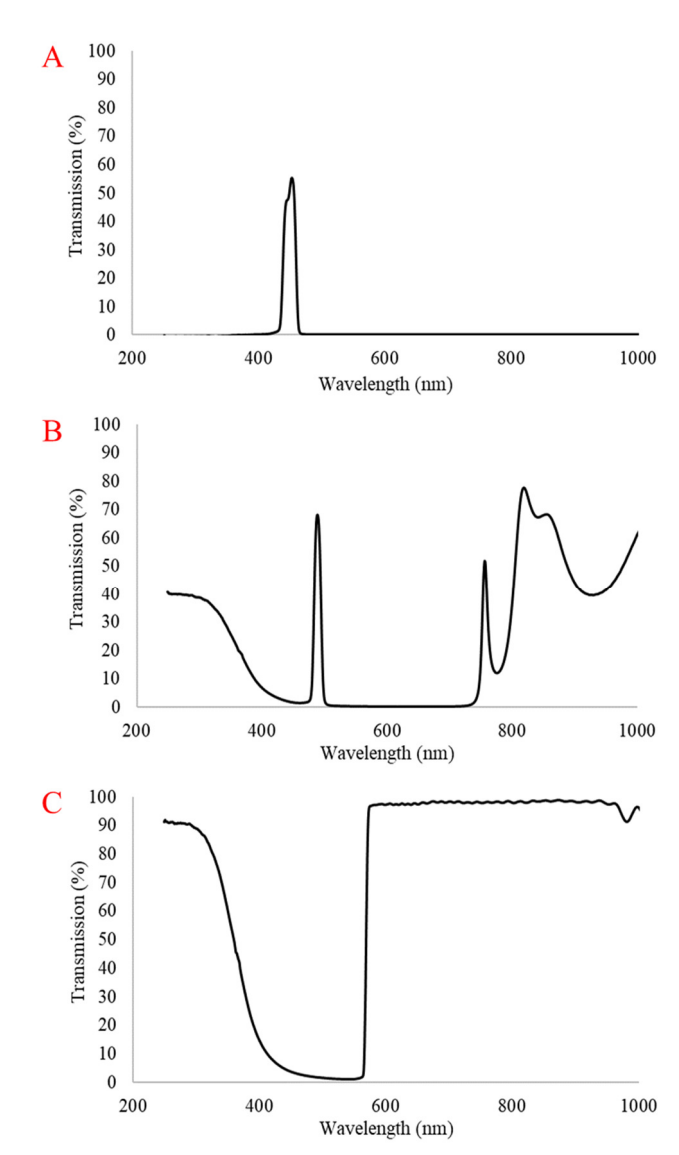


Figure 1: Transmission spectrum of the filters used for fluorescence imaging: (A) 450 nm band-pass filter, (B) 488 nm band-pass filter and (C) 570 nm long-pass filter.

Results from optical filter measurements indicate the importance to characterize the transmission of optical components used in the design of any spectral imaging system. For example, the 488 band-pass filter (Figure 1.B) has some unique transmission peaks in the IR region. Fortunately, these did not present an issue as the excitation sources are below the 488 nm cut-off. Ideally, the long-pass filter (Figure 1.C) should have 0% transmission to the left of the cut-off, but in the case of the 570 nm filter there was a large amount of transmission below 400 nm. Each filter was placed in the endoscopic light path before the camera detector and used as the emission filter for fluorescence imaging of the FSK5 fluorescent slides. However, prior to imaging, the transmission of the fluorescence test slides was measured (Figure 2) with the spectrometer setup described above.

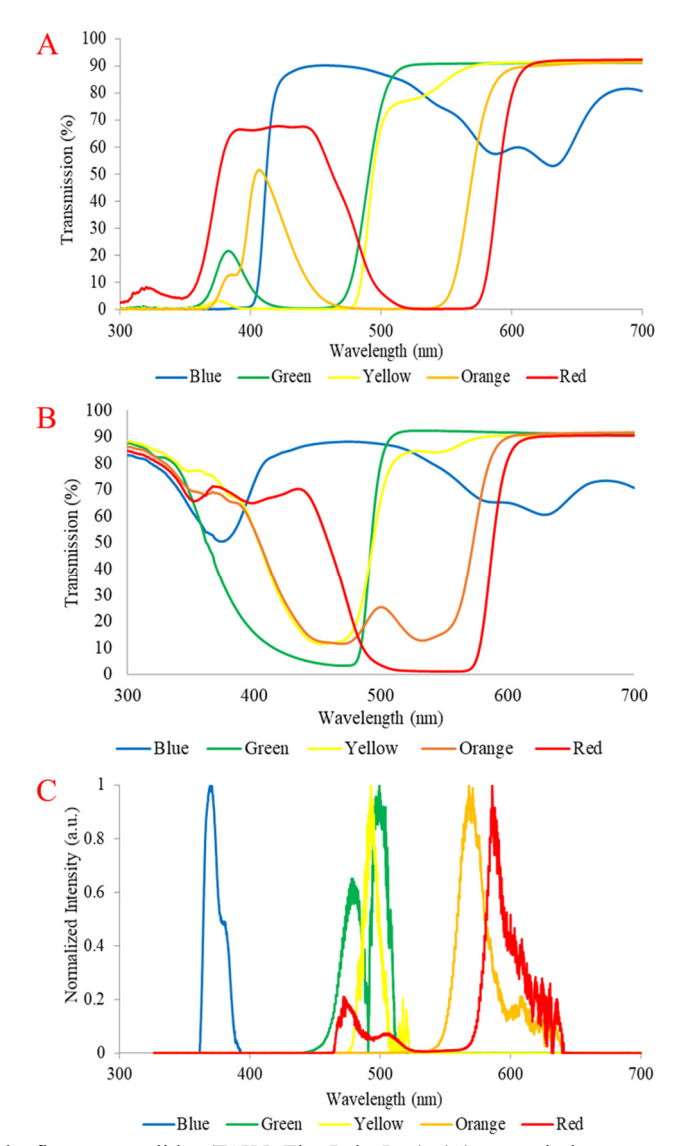


Figure 2: Irradiance data for the fluorescent slides (FSK5, ThorLabs Inc.): (A) transmission spectra for each slide provided by the manufacturer, (B) measured transmission spectra for comparison to data provided in panel A and (C) fluorescence spectra for each slide provided by the manufacturer.

The results we acquired were in high agreement with the transmission data provided by the manufacturer above 400 nm. Below 400 nm, there was some variance in the measurements, but in the case of endoscopic imaging, ultraviolet illumination (below 350 nm) would likely not be used. For each band-pass filter, a subset of the LED array was used as the excitation in the fluorescence imaging tests (Table 2).

Table 2: The subset of LEDs illuminated in the LED array of the hyperspectral endoscope system paired with the band-pass filter used for fluorescence imaging.

Band-pass Filter	LED Array					
450 nm Short-pass	405 nm, 420 nm					
488 nm Short-pass	405 nm, 420 nm, 450 nm, 470 nm					
570 nm Long-pass	405 nm, 420 nm, 450 nm, 470 nm, 525 nm					

The LED illumination wavelength was coordinated with camera image acquisition using external TTL triggering. The relative optimal settings for these tests acquired an image at 1 s per wavelength so an image stack was acquired at 2 s, 4 s and 5 s respectively. These images were used to determine the emitted spectrum as a function of the excitation sources (LED wavelengths). Regions of interest (ROI) were drawn in 4 different sections of the fluorescent label image. The spectrum of each ROI was plotted then averaged for the fluorescent spectra for the entire image. Figure 3 provides spectral response of each slide for each of the different filter-LED array combinations.

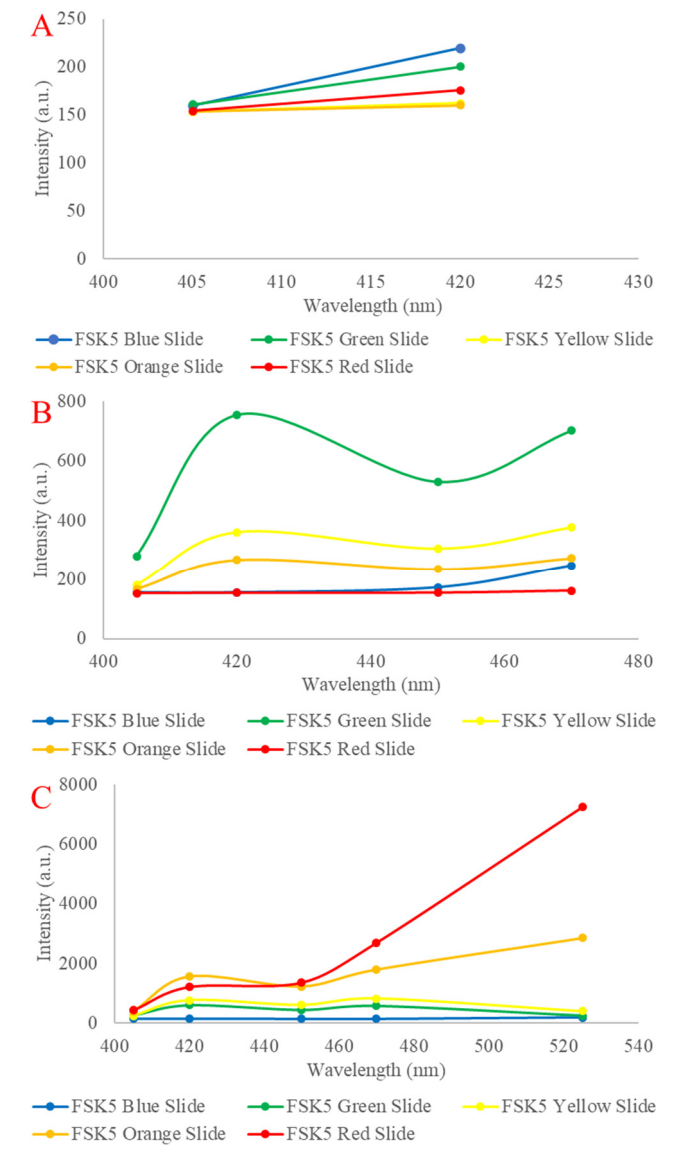


Figure 3: Fluorescence spectra as a function of excitation (LEDs) for each of the fluorescent slides using each band-pass filter. Fluorescence of each slide using (A) the 450/20 nm band-pass filter, (B) the 488/15 nm band-pass filter and (C) the 570 nm long-pass filter.

While highly qualitative, we believe this proves the feasibility of fluorescence imaging using this hyperspectral endoscopic platform. The graphs above show the emission intensity of each fluorescent slide as a function of the excitation LEDs illuminated. The emitted intensity is also a function of the emission peak of the slide (Figure 2.C), the transmission (or the inverse, absorbance) of the respective fluorescent slide (Figure 2.A-B) and the transmission of the band-pass filter used (Figure 1). The slide set imaged using the 450 nm band-pass filter (Figure 3.A) had the lowest accuracy due to only two data points (405 nm and 420 nm), yet the data was to be expected with the highest intensity from the blue and green slide (closest to the emission cut-off). Also, the overall intensity was lower because there were fewer excitation sources. Data

from the images using the 488 nm band-pass filter (Figure 3.B) presented similar trends with the notable peaks in the green slide fluorescence. The red and blue slide had the lowest absorbance (highest transmission, Figure 2.A-B) in this range which is verified by the two lowest curves on the 488 nm band-pass graph. Finally, the fluorescence data through the 570 nm long-pass filter (Figure 3.C) provide an initial indication of the feasibility of hyperspectral imaging in an endoscopic environment. Here, the red fluorescent slide emission was the highest intensity and subsequently the blue slide was the lowest. These data also showed the similarities in the yellow and green slide spectra. The intensity scale also reflected that a long-pass filter was used and higher number of LEDs were cycled through with the tenfold increase in intensity. Overall, fluorescence testing using the fluorescent slide set proved successful in showing the feasibility of the fluorescence hyperspectral imaging through an endoscope. This data will act as initial baseline testing for performance as this technology improves. These new fluorescent standards will allow for better understanding of the image data collected from an array of discreet bandwidths source with potentially differing excitation widths and spacing (spectral resolution).

#### 4. FUTURE WORK

Fluorescent testing will continue with a larger selection of band-pass filters, specifically long-pass filters and subsequently a larger array of LEDs. A larger array of fluorescent slides or labels will be imaged. Further testing of tissue samples will allow us to verify the standards mentioned above and continue to acquire mixed image data (reflectance and autofluorescence) to test the viability of the technique. Currently, the limiting factor in real-time hyperspectral imaging is the amount light or signal. We will continue to improve the light combining optics to maximize transmitted light.

## 5. ACKNOWLEDGEMENTS

The authors would like to acknowledge support from the NASA/Alabama Space Grant Consortium, NASA Grant #NNX15AJ18H, NIH grant numbers UL1 TR001417, P01 HL066299, NSF grant number 1725937, the Abraham Mitchell Cancer Research Fund, the University of Alabama at Birmingham Center for Clinical and Translational Science (CCTS), and the Economic Development Partnership of Alabama. Drs. Leavesley and Rich disclose financial interest in a start-up company, SpectraCyte LLC, founded to commercialize spectral imaging technologies.

#### REFERENCES

- [1] Leskosky, R.J., "Phenakiscope: 19th Century Science Turned to Animation," Film History 5(2), 176–189 (1993).
- [2] Braun, M., [Picturing Time: The Work of Etienne-Jules Marey (1830-1904)], University of Chicago Press (1994).
- [3] Davidson, M.W., "Pioneers in Optics: Étienne-Jules Marey and Ignazio Porro," Microscopy Today 18(5), 44–46 (2010).
- [4] Spehr, P., [The Man Who Made Movies: W.K.L. Dickson], Indiana University Press (2008).
- [5] BAGGETT, P., "Review of Literature and Photography in Transition, 1850–1915," Studies in American Naturalism 11(2), 84–88 (2016).
- [6] Ignjatovic, A., East, J., Guenther, T., Hoare, J., Morris, J., Ragunath, K., Shonde, A., Simmons, J., Suzuki, N., et al., "What is the most reliable imaging modality for small colonic polyp characterization? Study of white-light, autofluorescence, and narrow-band imaging.," Endoscopy 43(2), 94–99 (2011).
- [7] Chiu, H.-M., Chang, C.-Y., Chen, C.-C., Lee, Y.-C., Wu, M.-S., Lin, J.-T., Shun, C.-T., and Wang, H.-P., "A prospective comparative study of narrow-band imaging, chromoendoscopy, and conventional colonoscopy in the diagnosis of colorectal neoplasia," Gut 56(3), 373–379 (2007).
- [8] Li, Y.-H., Yue, J.-C., and Cai, G.-P., "Fluorescence characterization of type I collagen from normal and silicotic rats and its quenching dynamics induced by hypocrellin B," Biopolymers 42(2), 219–226 (1997).
- [9] Fang, M., Yuan, J., Peng, C., and Li, Y., "Collagen as a double-edged sword in tumor progression," Tumour Biology 35(4), 2871–2882 (2014).

- [10] Deyl, Z., Macek, K., Adam, M., and Vančíková, "Studies on the chemical nature of elastin fluorescence," Biochimica et Biophysica Acta (BBA) Protein Structure 625(2), 248–254 (1980).
- [11] Puchtler, H., Waldrop, F.S., and Valentine, L.S., "Fluorescence microscopic distinction between elastin and collagen," Histochemie 35(1), 17–30 (1973).
- [12] Skala, M.C., Riching, K.M., Gendron-Fitzpatrick, A., Eickhoff, J., Eliceiri, K.W., White, J.G., and Ramanujam, N., "In vivo multiphoton microscopy of NADH and FAD redox states, fluorescence lifetimes, and cellular morphology in precancerous epithelia," Proceedings of the National Academy of Sciences 104(49), 19494–19499 (2007).
- [13] Galbán, J., Sanz-Vicente, I., Navarro, J., and de Marcos, S., "The intrinsic fluorescence of FAD and its application in analytical chemistry: a review," Methods and Applications in Fluorescence 4(4), 042005 (2016).
- [14] Schaefer, P.M., Kalinina, S., Rueck, A., Arnim, C.A.F. von, and Einem, B. von, "NADH Autofluorescence—A Marker on its Way to Boost Bioenergetic Research," Cytometry Part A 95(1), 34–46 (2019).
- [15] Krieg, R.C., Messmann, H., Rauch, J., Seeger, S., and Knuechel, R., "Metabolic Characterization of Tumor Cell–specific Protoporphyrin IX Accumulation After Exposure to 5-Aminolevulinic Acid in Human Colonic Cells"," Photochemistry and Photobiology 76(5), 518–525 (2002).
- [16] de Oliveira Silva, F.R., Bellini, M.H., Tristão, V.R., Schor, N., Vieira, N.D., and Courrol, L.C., "Intrinsic Fluorescence of Protoporphyrin IX from Blood Samples Can Yield Information on the Growth of Prostate Tumours," Journal of Fluorescence 20(6), 1159–1165 (2010).
- [17] Lisy, M.-R., Goermar, A., Thomas, C., Pauli, J., Resch-Genger, U., Kaiser, W.A., and Hilger, I., "In Vivo Near-infrared Fluorescence Imaging of Carcinoembryonic Antigen–expressing Tumor Cells in Mice," Radiology 247(3), 779–787 (2008).
- [18] Betz, C.S., Stepp, H., Janda, P., Arbogast, S., Grevers, G., Baumgartner, R., and Leunig, A., "A comparative study of normal inspection, autofluorescence and 5-ALA-induced PPIX fluorescence for oral cancer diagnosis," International Journal of Cancer 97(2), 245–252 (2002).
- [19] Mulla, D.J., "Twenty five years of remote sensing in precision agriculture: Key advances and remaining knowledge gaps," Biosystems Engineering 114(4), 358–371 (2013).
- [20] Cavalli, R.M., Licciardi, G.A., and Chanussot, J., "Detection of anomalies produced by buried archaeological structures using nonlinear principal component analysis applied to airborne hyperspectral image," IEEE Journal of Selected Topics in Applied Earth Observations and Remote Sensing 6(2), 659–669 (2013).
- [21] Sun, D.-W., [Hyperspectral imaging for food quality analysis and control], Elsevier (2010).
- [22] Goltz, D., Attas, M., Young, G., Cloutis, E., and Bedynski, M., "Assessing stains on historical documents using hyperspectral imaging," Journal of cultural heritage 11(1), 19–26 (2010).
- [23] Bauriegel, E., Giebel, A., and Herppich, W.B., "Hyperspectral and chlorophyll fluorescence imaging to analyse the impact of Fusarium culmorum on the photosynthetic integrity of infected wheat ears," Sensors 11(4), 3765–3779 (2011).
- [24] Lim, H.-T., and Murukeshan, V.M., "A four-dimensional snapshot hyperspectral video-endoscope for bio-imaging applications," Scientific Reports 6(1), 1–10 (2016).
- [25] Gao, L., Kester, R.T., Hagen, N., and Tkaczyk, T.S., "Snapshot Image Mapping Spectrometer (IMS) with high sampling density for hyperspectral microscopy," Optics Express 18(14), 14330 (2010).
- [26] Favreau, P.F., Hernandez, C., Heaster, T., Alvarez, D.F., Rich, T.C., Prabhat, P., and Leavesley, S.J., "Excitation-scanning hyperspectral imaging microscope," Journal of biomedical optics 19(4), 046010–046010 (2014).
- [27] Browning, C.M., Mayes, S., Favreau, P., Rich, T.C., and Leavesley, S.J., "LED-based endoscopic light source for spectral imaging," presented at SPIE BiOS, 2016, 97031I-97031I.

- [28] Browning, C.M., Mayes, S., Rich, T.C., and Leavesley, S.J., "Design of a modified endoscope illuminator for spectral imaging of colorectal tissues," presented at Proc. of SPIE Vol, 2017, 1006015–1.
- [29] Browning, C.M., Mayes, S., Rich, T.C., and Leavesley, S.J., "Endoscopic hyperspectral imaging: light guide optimization for spectral light source," presented at Multimodal Biomedical Imaging XIII, 2018, 104870H.
- [30] Browning, C.M., Mayes, S., Deal, J., Arshad, A., Mayes, S.G., Parker, M., Rich, T.C., and Leavesley, S.J., "Sensitivity analysis of a multibranched light guide for real time hyperspectral imaging systems," presented at Multimodal Biomedical Imaging XIV, 2019, 1087107.
- [31] Browning, C.M., Deal, J., Mayes, S., Arshad, A., Rich, T.C., and Leavesley, S.J., "Excitation-scanning hyperspectral video endoscopy: enhancing the light at the end of the tunnel," Biomedical Optics Express 12(1), 247 (2021).